Environmental Technology & Innovation 40 (2025) 104423

Contents lists available at ScienceDirect

Environmental Technology & Innovation

journal homepage: www.elsevier.com/locate/eti

Mg-modified biochar increases adsorption and retention of nitrogen and phosphorus in greenhouse vegetable soil

Yaling Wang [a,b,1], Yuyang Cheng [b,c,1], He Wang [a], Zhengping Peng [a], Xinyue Wen [b], Xiuwen Mei [b], Chunjing Liu [a,*], Xiubin Wang [b,*]

[a] College of Resources and Environmental Sciences, Hebei Agricultural University, Baoding 071000, PR China
[b] State Key Laboratory of Efficient Utilization of Arable Land in China, the Institute of Agricultural Resources and Regional Planning, Chinese Academy of Agricultural Sciences, Beijing 100081, PR China
[c] Hubei Provincial Engineering Research Center of Efficient Utilization of Nutrient Resources, Xinyangfeng Agricultural Technology Co. Ltd, Jingmen, Hubei 448000, PR China

ARTICLE INFO

Keywords:
Mg-modified biochar
Nitrogen/phosphorus
Adsorption
Retention
Greenhouse vegetable soil

ABSTRACT

High accumulation of nitrogen (N) and phosphorus (P) in greenhouse vegetable soils raises leaching risks. Metal-modified biochar can enhance soil adsorption of either N or P, but its adsorption and retention effects under the addition of dual-solute (N and P) remain unclear. In this study, raw biochar (BC) was prepared by pyrolyzing sheep manure at 550°C under N_2 atmosphere, while Mg-modified biochar (Mg-BC) was synthesized by mixing BC with 0.5 mol L^{-1} $MgCl_2$. Adsorption isotherms, soil column leaching, and pot experiments were conducted to explore their effects on the adsorption and retention of N and P in greenhouse vegetable soil under co-existing addition of N and P solutes. Results showed that the Mg-BC treatment contained more surface oxygen-containing groups and $MgO/Mg(OH)_2$ crystals. According to the Langmuir model, the maximum adsorption capacities of Mg-BC for NO_3^- and PO_4^{3-} were 1.38 and 1.84 times those of BC, respectively. Soil column leaching experiments showed that the Mg-BC treatment reduced total N and P leaching losses by 30.98 % and 51.25 % compared to BC, effectively inhibiting NO_3^--N, dissolved inorganic N, and soluble reactive P leaching. Additionally, compared to BC, Mg-BC increased pakchoi biomass by 17.28 % and enhanced soil NO_3^--N, ammonium N, and available P (AP) by 128.22 %, 44.67 %, and 52.94 %, respectively. Overall, Mg-BC exhibits dual functions in N/P adsorption and nutrient availability enhancement, guiding future research on optimizing modified biochar and promoting sustainable greenhouse vegetable production.

1. Introduction

A prevalent practice in greenhouse vegetable cultivation was the overuse of nitrogen (N) and phosphorus (P) fertilizers (Guo et al., 2025a; Kalkhajeh et al., 2017), leading to high accumulation of N and P in soils and posing environmental risks (Kalkhajeh et al., 2021). Among these, nitrate (NO_3^-) and phosphate (PO_4^{3-}) leaching were the main forms of water contamination (Li et al., 2024b;

* Corresponding authors.
E-mail addresses: chunjingliu2008@163.com (C. Liu), wangxiubin@caas.cn (X. Wang).
[1] Yaling Wang and Yuyang Cheng contributed equally to this work and should be considered co-first authors.

https://doi.org/10.1016/j.eti.2025.104423
Received 27 May 2025; Received in revised form 12 July 2025; Accepted 2 August 2025
Available online 5 August 2025

Wang et al., 2020), their adsorption capacity by soil colloids was limited and significantly influenced by pH and ionic strength (Xu et al., 2016). Developing functional materials with high adsorption affinity and long-term retention capacity to enhance soil N and P immobilization, reduce leaching risks, and improve soil nutrient availability held dual significance for controlling agricultural non-point source pollution and promoting efficient nutrient resource utilization (Fang et al., 2020; Sui and Dai, 2025; Weng et al., 2018; Zhang et al., 2025b).

Biochar, as an efficient adsorbent, effectively adsorbed cations such as NH_4^+, Ca^{2+}, and K^+ (Adelawon et al., 2021; Muema et al., 2024; Peng et al., 2011), but its adsorption capacity for anions like NO_3^- and PO_4^{3-} was limited (Mahmoud et al., 2024; Sun et al., 2022). To enhance the adsorption performance and selectivity of biochar, metal-modified biochar showed promising application prospects (Guo et al., 2025b; Oginni et al., 2020; Qin et al., 2023). Previous research demonstrated that the adsorption capacity of metal-modified biochar for NO_3^- and PO_4^{3-} in water significantly improved compared to unmodified biochar (Chandra et al., 2020; Tang et al., 2025; Wu et al., 2024). Moreover, several studies were conducted on the adsorption of NO_3^-or PO_4^{3-} in soil using metal-modified biochar. For instance, Gu et al. (2023) found that iron-modified biochar adsorbed 1.32 and 4.80 times more NH_4^+ and NO_3^-, respectively, in black soil than raw biochar. Wu et al. (2019) reported that MgO-modified biochar achieved an adsorption capacity of 18.94 mg g^{-1} for PO_4^{3-} in saline-alkali soil, which was 1.46 times that of raw peanut shell biochar. However, few studies had reported the adsorption performance of metal-modified biochar for both soil NO_3^- and PO_4^{3-} in N-P dual-solute systems.

Numerous studies indicated that biochar generally reduced N and P leaching loss in soil (Sun et al., 2024; Zhang et al., 2021, 2023). With the emergence of metal-modified biochar, its effectiveness in controlling the leaching loss of N and P in soil attracted widespread attention. Compared to raw biochar, the application of Mg-modified corn straw biochar decreased NO_3^- concentrations in leachate from open-field vegetable plots by 3.9 %–30.2 % (Zhou et al., 2024). Metal-modified biochar showed either inhibitory effects (Peng et al., 2021; Wu et al., 2020) or no significant influence (Riddle et al., 2018) on P leaching. This difference could be attributed to the variations in soil types, experimental durations, biomass materials, types of loaded metals, and their application dosages (Wu et al., 2020; Zheng et al., 2020). Given that high accumulation of N and P in protected vegetable soils led to increased leaching risks, it was particularly important to systematically investigate how metal-modified biochar efficiently controlled N and P leaching.

Simultaneously, metal-modified biochar demonstrated significant value in enhancing soil N/P retention and nutrient availability. For N regulation, Mg-BC reduced N leaching by 50.48 % via strengthened electrostatic adsorption and pore interception, with its surface functional groups sustaining stable N supply (Zhou et al., 2024). Ibrahim et al. (2023) noted that Mg-O modified biochar increased soil NO_3^--N content by 21.92 % through mitigating NO_3^- loss. In P management, Fe-Al and Mg-Al bimetal-modified biochars boosted long-term P supply by regulating the transformation of P forms (Peng et al., 2023). Wu et al. (2020) revealed that Fe(II)-BC, with abundant high-active sites, achieved a maximum P adsorption capacity of 39.2 mg g^{-1}, increasing AP in saline-alkali soils by 78.6 %. Moreover, metal-modified biochar improved crop productivity. For example, magnetic modification increased AP in degraded black soils by 51.52 % and soybean yield by 17.48 % (Gong et al., 2024). Mg-BC enhanced Chinese cabbage growth, increasing its fresh weight and N uptake by 164.73 % and 201.29 %, respectively (Zhou et al., 2024). These effects stemmed from synergies in improving nutrient supply and optimizing rhizosphere microbial communities (Peng et al., 2023; Zhang et al., 2025a). However, most studies focused on single nutrients or open-field environments, remaining unclear in exploring how metal-modified biochar synergistically regulated nutrient availability and crop responses in greenhouse systems with co-enrichment of N and P.

Among metal-modified biochars, Fe/Al-modified variants showed strong anion adsorption (notably in acidic-neutral soils) but faced limitations: over-application risked phytotoxicity (Ahmed et al., 2024; Wei et al., 2024). In contrast, Mg-BC offered distinct advantages. It displayed excellent anion exchange capacity, efficiently capturing target ions even with multiple coexisting anions. Critically, it supplied utilizable Mg to plants, posed no leaching toxicity, and synergistically enhanced soil quality and fertility (Ahmed et al., 2024; Cao et al., 2019). A key strength was its behavior during N and P adsorption: Mg-BC formed stable slow-release complexes like struvite ($MgNH_4PO_4{\cdot}6H_2O$), balancing nutrient retention and plant supply (Gu et al., 2025; Ibrahim et al., 2023). This avoided the "adsorb-only, no-supply" flaw of Fe/Al-modified biochars (Datta et al., 2015; Li et al., 2021). Thus, Mg-BC emerged as an efficient and eco-friendly ideal for agricultural N-P synergistic management. Moreover, Livestock manure, as a bulk agricultural waste, could lead to resource wastage and environmental pollution if improperly handled (Mehmood et al., 2017). Among these, sheep manure was characterized by its high fiber content, low P levels, and slow decomposition rate, which contributed to improved soil aeration, water retention, and nutrient-holding capacity (Freschet et al., 2008; Macholdt et al., 2019).Therefore, this study selected sheep manure to prepare both raw and Mg-modified biochar, with greenhouse vegetable soil as the experiment substrate and pakchoi (*Brassica chinensis* L.) as the experiment crop. The objectives were: (i) to evaluate the adsorption capacity of Mg-modified biochar for NO_3^- and PO_4^{3-} in greenhouse vegetable soil, (ii) to determine its inhibitory effect on soil N and P leaching, and (iii) to elucidate its impacts on soil N and P availability, pakchoi biomass, and nutrient uptake. We hypothesized that Mg-modified biochar would enhance the adsorption and retention of N and P in greenhouse vegetable soil, thereby increasing soil N/P availability, promoting nutrient uptake by pakchoi, and improving biomass.

2. Materials and methods

2.1. Preparation of biochar and soil sample

The raw material, sheep manure, was provided by Xihong Township, Zhumadian City, Henan Province, China. The composted materials were crushed into particles under 5 mm. Samples were heated in a microwave muffle furnace (SX2) from room temperature to 550°C at 10°C per minute. The process, conducted by Shanghai Rongfeng Scientific Instrument Inc., operated under an N_2 atmosphere. After reaching 550°C, the temperature was maintained for 2 h, followed by cooling to obtain raw biochar (BC). The BC was

mixed with 0.5 mol L^{-1} $MgCl_2$ solution at a 1:20 g mL^{-1} ratio. The pH was adjusted to 8.0 using 1.0 mol L^{-1} NaOH. The mixture was incubated at 85℃ for 48 h, then filtered, washed with deionized water, and dried at 105°C. The resulting Mg-modified biochar (Mg-BC) was ground into particles below 2 mm for further use, following Zheng et al. (2020). Table 1 summarizes the properties of sheep manure, BC, and Mg-BC.

Soil samples (0–20 cm depth) were collected from a greenhouse vegetable field in Wuqing District, Tianjin, China (39°56′N, 116°98′E), derived from fluvo-aquic soils. The samples were air-dried naturally at room temperature and sieved through a 2 mm mesh. The fundamental soil physicochemical included pH 7.17, organic matter 25.25 g kg^{-1}, total N (TN) 1.65 g kg^{-1}, total P (TP) 2.12 g kg^{-1}, NO_3^--N 25.04 mg kg^{-1}, ammonium N (NH_4^+-N) 7.32 mg kg^{-1}, AP 223.97 mg kg^{-1}, available K 492.42 mg kg^{-1}.

2.2. Characterization of BC and Mg-BC samples

The Mg-BC sample underwent Fourier Transform-Infrared spectroscopy analysis (FTIR, Thermo iS20, USA) using the KBr pellet method. Samples were pretreated with KBr pellets and analyzed for surface functional groups after achieving uniform pellet formation. The surface morphology was examined by scanning electron microscope and an energy dispersive spectrometer (SEM-EDS, Hitachi S4800, Japan). The specimens were mounted on conductive adhesive tape, sputter-coated, and imaged at 10 kV using high-resolution SEM. Furthermore, Elemental composition was quantified through EDS surface scanning. X-ray diffraction patterns were obtained using an XRD instrument (Panalytical Empyrean, Netherlands) with Cu Kα radiation (40 kV, 100 mA), scanning a 2θ range of 10°−80° at 2°/min. The changes of elemental valence states on BC materials were measured by X-ray photoelectron spectroscope (XPS, Escalab Xi+, USA).

2.3. NO_3^- and PO_4^{3-} adsorption in greenhouse vegetable soil

The adsorption experiments were conducted with three different treatments: CK (control without biochar), BC, and Mg-BC, each containing 1 % biochar (mass percentage, w/w). For each treatment, 2.5 g of soil-biochar mixture was added to a 50 mL centrifuge tube. To simulate the co-existing conditions of $NO_3^-$and PO_4^{3-}, mixed solutions were prepared using KNO_3 and KH_2PO_4. Both NO_3^- and PO_4^{3-} concentrations in the solutions were established with gradients ranging from 0 to 1000 mg L^{-1} , specifically at the following concentration points: 0, 20, 40, 60, 80, 100, 160, 200, 300, 400, 600, 800, and 1000 mg L^{-1} . A 25 mL aliquot of each solution was added to the tubes, with 0.01 mol L^{-1} KCl as the background electrolyte. Chloroform (1–2 drops) was added to suppress microbial growth. Samples were shaken at 180 rpm for 24 h (25°C), centrifuged (4000 rpm, 8 min), and filtered through a 0.45 μm membrane. All steps were performed in triplicate. NO_3^- and PO_4^{3-} concentrations in the filtrate were measured using continuous flow analysis-N-(1-naphthyl) ethylenediamine dihydrochloride spectrophotometry) and molybdenum-antimony anti-spectrophotometry, respectively. Adsorption data of N and P were calculated using the difference between initial and equilibrium concentrations. The N and P adsorption capacity can be calculated using the following formula:

$$q_e = \frac{(C_o - C_e)V}{m} \tag{1}$$

where C_0 (mg L^{-1}) and C_e (mg L^{-1}) represent the initial and equilibrium NO_3^- (PO_4^{3-}) concentrations, respectively; m (g) represents the weight of the absorbent; and V (L) represents the volume of the NO_3^- (PO_4^{3-}) solution.

The Langmuir (Eq. 2) and Freundlich (Eq. 3) models were fitted to the adsorption data to estimate theoretical maximum adsorption capacities for N and P:

$$Q_e = \frac{K_L Q C_e}{(1 + K_L C_e)} \tag{2}$$

$$Q_e = K_f {C_e}^{1/n} \tag{3}$$

where K_L (L mg^{-1}) and K_f ($mg^{(1-n)}$ L^n g^{-1}) are the Langmuir and Freundlich constants, respectively; Q denotes the Langmuir maximum adsorption capacity (mg g^{-1}); Ce represents the equilibrium solution concentration (mg L^{-1}); and n is the Freundlich linearity constant.

2.4. Leaching experiments in the BC and Mg-BC amended soils

This study investigated N and P leaching in greenhouse vegetable soil using a soil column method (Zheng et al., 2020). Three

Table 1
The basic properties of sheep manure derived biochar (BC) and Mg-modified biochar (Mg-BC) used in this study.

Types	Surface area (m^2 g^{-1})	C (%)	H (%)	O (%)	N (%)	P (%)	K (%)	Mg (%)	pH	Organic matter (%)
Mg-BC	6.63	7.90	3.02	16.32	0.36	2.82	1.52	4.82	9.10	-
BC	5.28	12.42	0.78	7.15	0.77	2.64	2.35	0.68	10.42	-
Manure	-	-	-	-	1.71	1.19	2.18	-	7.70	37.40

treatments were tested: control (CK), BC, and Mg-modified biochar (Mg-BC, each with three replicates. BC and Mg-BC were mixed into soil at 1 % (w/w). The composite soil-biochar samples were partitioned into two sections (300 g and 100 g) and encapsulated within an acrylic cylinder featuring an internal diameter of 5 cm, the structure stands at a towering 25 cm, featuring tiny perforations at its base. Prior to filling, a 100-mesh nylon filter was positioned at the base of the column, and a layer of 2 cm thickness, acid-washed quartz sand was incorporated to facilitate the even distribution of water flow. Subsequently, 300 g of a composite soil sample were incorporated as the base layer. Proportionately blend 0.0848 g of potassium dihydrogen phosphate with 0.1890 g of urea as the N and P fertilizer into the upper mixed soil, respectively. Ultimately, top it off with a 2 cm thick layer of quartz sand. Proceed by adding deionized water to the soil column until it reaches saturation, and allow the saturated soil column to incubate for a period of 2 days prior to initiating leaching.

Thereafter, a 100 mL aliquot of deionized water was incorporated every 3 days over a 21-day duration. Leachates were collected for N and P in different forms analysis. The leachate samples underwent direct analysis for TN content was measured directly using a Multi N/C 3100/HT1300 spectrophotometer (Analytik Jena AG, Germany). NO_3^--N and NH_4^+-N concentrations were determined after filtration through a 0.45 μm membrane using a continuous flow analyzer (SEAL Auto Analyzer 3). The dissolved inorganic N (DIN) was calculated based on this sum. Total dissolved nitrogen (TDN) was analyzed post-filtration (0.45 μm membrane) using a Multi N/C 3100/HT1300 analyzer. The difference between TDN and DIN represents the concentration of dissolved organic N (DON). TP in leachate was measured using $K_2S_2O_8$ digestion. Leachate samples were filtered through a 0.45 μm membrane immediately after collection, and the filtrate was analyzed for soluble reactive phosphorus (SRP). To determine total soluble phosphorus (TSP), the same filtrate underwent $K_2S_2O_8$ digestion before measurement. Particulate phosphorus (PP) was calculated as TP minus TSP, while soluble organic phosphorus (SOP) was derived by subtracting SRP from TSP.

2.5. Effect of BC and Mg-BC on soil available N and P content, nutrient uptake and pakchoi biomass

The pot experiment was conducted in a greenhouse at the Chinese Academy of Agricultural Sciences. Three treatments were tested in a randomized block design with three replicates each: (1) CK, no biochar; (2) BC and (3) Mg-BC. The proportion of $N:P_2O_5:K_2O$ in the application was 7:1:6. Specific application rates were N: 150 kg ha^{-1} (urea: 1.02 g per pot), P_2O_5: 21 kg ha^{-1} (monopotassium phosphate: 0.13 g per pot), and K_2O: 126 kg ha^{-1} (potassium sulfate: 0.45 g per pot, adjusted for 34 % K_2O contribution from monopotassium phosphate), respectively. Air-dried soil (3.0 kg) was mixed uniformly with fertilizers and biochar, then placed into bottomless plastic containers. Twenty seeds of pakchoi (*Brassica chinensis* L., Yurun variety) were sown per pot. Seedlings were thinned

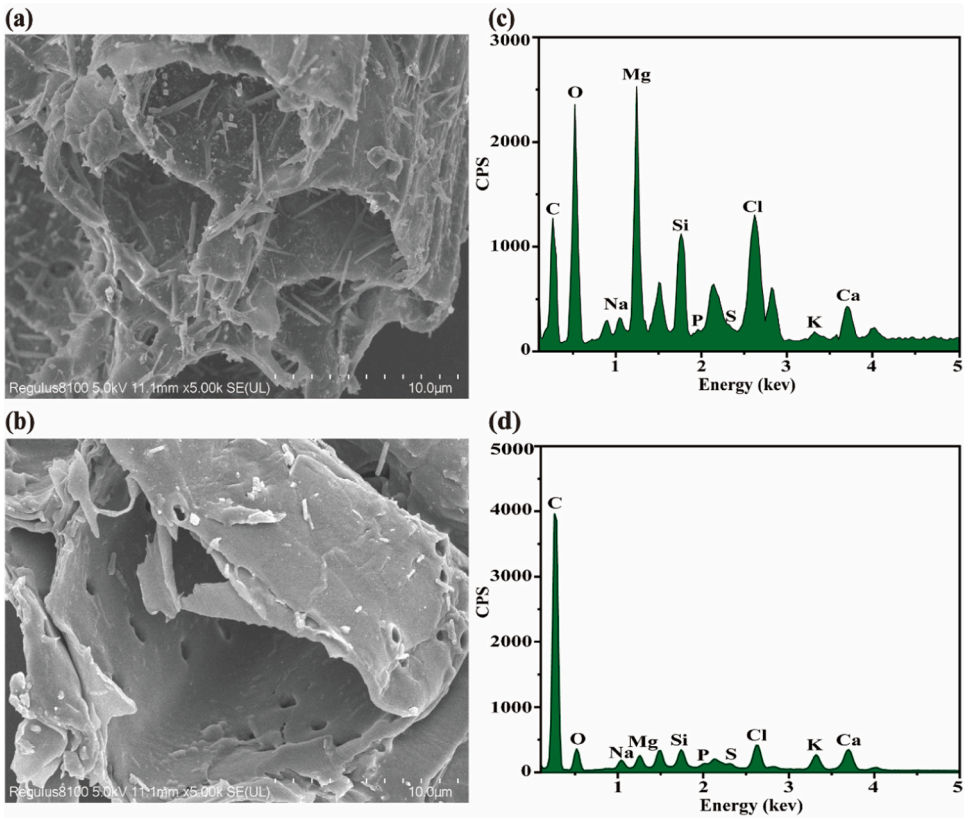

Fig. 1. SEM images of (a) Mg-BC (Mg-modified biochar) and (b) BC (raw biochar). EDS analyses of (c) Mg-BC and (d) BC. Bar= 10 μm.

to four plants per pot after true leaf development. Plants were grown in a sunlight greenhouse under controlled conditions: day/night average temperature at 25 ± 2°C, 12 h light/12 h dark photoperiod, and 50 % relative humidity. For consistent water management, pots were weighed before each irrigation, and deionized water was added to maintain soil moisture at 70 % field capacity throughout the growth period. Fresh weight was recorded immediately after harvest. Plant samples were oven-dried at 60°C, weighed, and analyzed for N, P, and K content (Haefele et al., 2011). Nutrient uptake was calculated by multiplying plant biomass by nutrient concentrations. Fresh soil subsamples were stored at 4°C for NO_3^--N and NH_4^+-N determination using a continuous flow analyzer. Air-dried soil was sieved (1 mm) for analysis: AP was extracted with 0.5 mol L^{-1} $NaHCO_3$ solution (pH 8.5) and measured using the molybdenum-antimony colorimetric method at a soil-to-solution ratio of 1:20. The determination of TN was achieved through the utilization of a Multi N/C 3100/HT1300 analyzer, as per the methodology employed. The estimation of TP was conducted on from soil samples that were digested with H_2SO_4 and $HClO_4$ as described (Wei et al., 2017).

2.6. Data analysis

The information gathered from the experimental trials was subjected to analysis utilizing both Excel 2019 and Origin 2022 software. The SPSS 23.0 software was utilized to perform the statistical analysis. Variations in different therapeutic approaches were investigated using a one-way analysis of variance (ANOVA), with statistical significance determined at a threshold of $P < 0.05$.

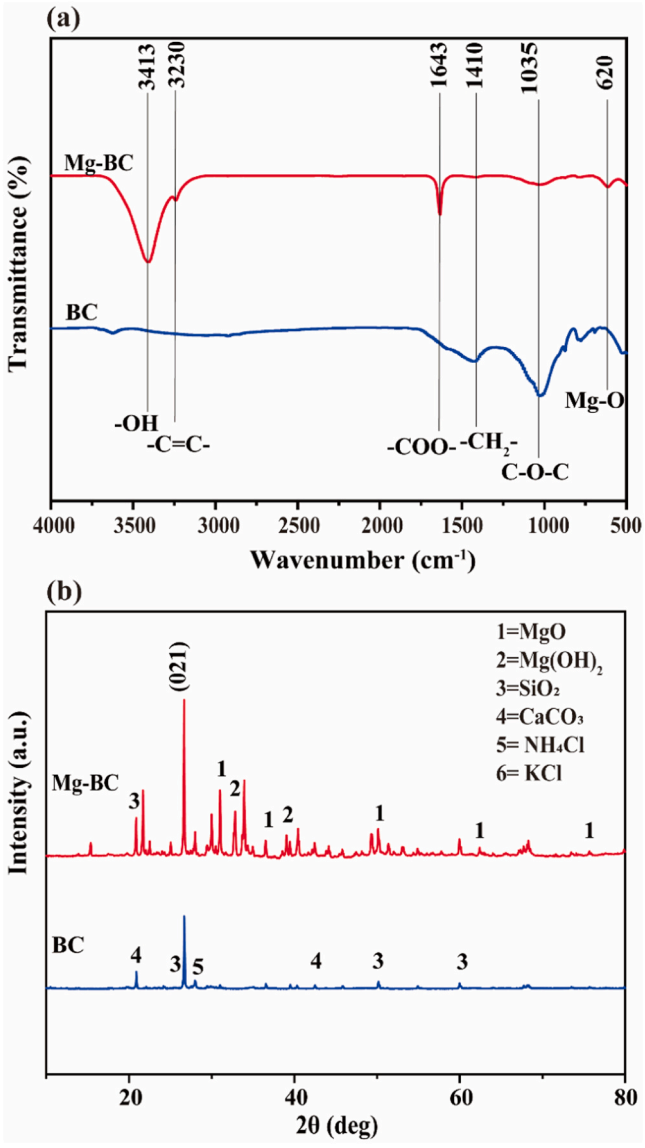

Fig. 2. (a) FTIR spectra of the BC (raw biochar) and Mg-BC (Mg-modified biochar), and (b) XRD patterns of the BC and Mg-BC.

3. Results

3.1. Characteristics of BC and Mg-BC

SEM is mainly used to reflect the changes in the surface morphological structure of biochar (Fig. 1). The surface of the raw biochar is generally smooth (Fig. 1b). However, after being modified by Mg^{2+}, the surface of the samples is relatively rough, and there are substances in the form of white particles and acicular substances attached to both the surface and inner walls of the pores (Fig. 1a).

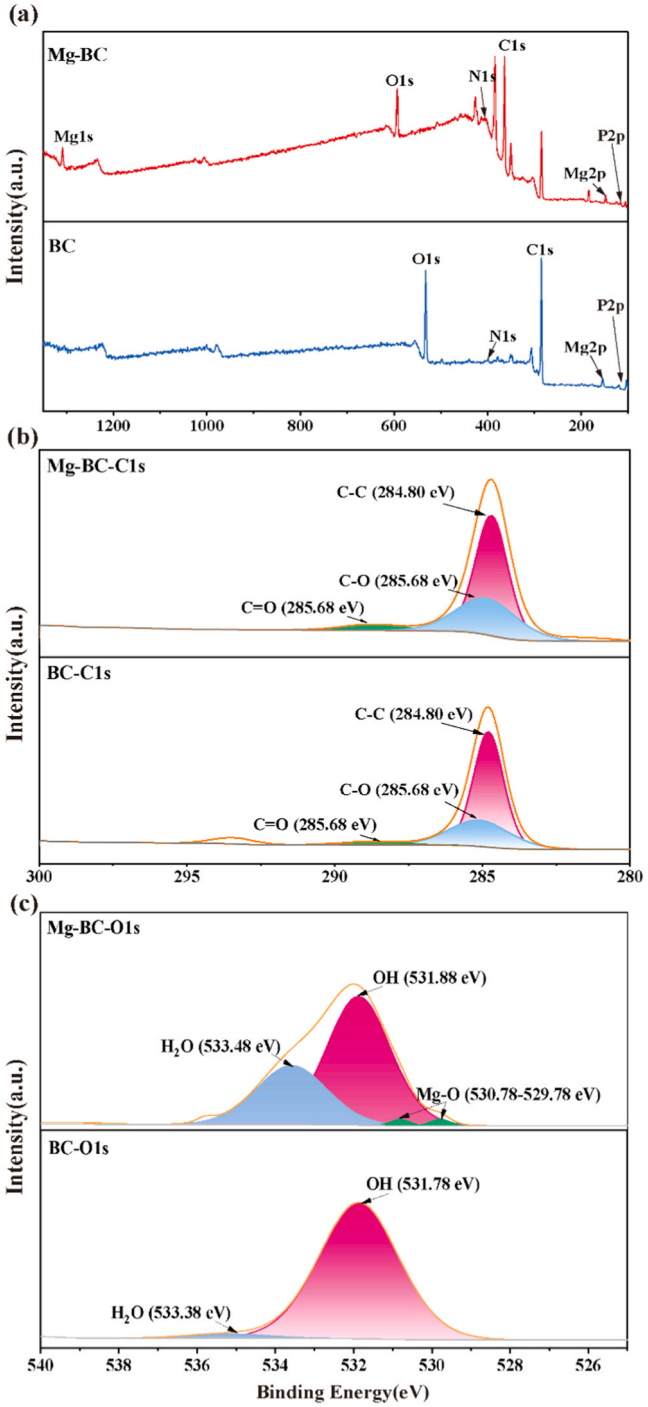

Fig. 3. XPS full spectra (a) and the high-resolution XPS spectra of C1s (b) and O1s (c) of the BC (raw biochar) and Mg-BC (Mg-modified biochar).

Such changes in appearance suggest that Mg might be bonded to the surface of the biochar. In addition, EDS analysis revealed that Mg-BC showed reduced C content, elevated O content, and a notable 28.31 % increase in Mg content relative to BC (Fig. 1c and d).

We employed FTIR spectroscopy to examine biochar samples, aiming to discern functional groups present in both Mg-BC and BC (Fig. 2a). The Mg-BC and BC performed characteristic absorption peaks corresponding to the stretching vibrations of -CH_2, C-O-C, and carboxyl group (-COO) respectively at different wavebands such as 1410 cm^{-1} , 1035 cm^{-1} , and 1643 cm^{-1} . However, the peak intensities of Mg-BC at the wavebands of 1410 cm^{-1} and 1035 cm^{-1} were relatively weak, and it was clearly found that after Mg^{2+} modification, the peak intensity in this waveband at 1643 cm^{-1} (-COO), 3413 cm^{-1} (-OH), and 3230 cm^{-1} (-C═O) was enhanced. Mg-BC showed characteristic absorption peaks different from those of BC in the waveband ranges of 620 cm^{-1} (Mg-O).

Moreover, XRD confirmed the successful loading of Mg^{2+} onto the Mg-BC (Fig. 2b). The Mg-modified biochar presents the unique diffraction peaks of Mg chloride, that is, the (021) crystal planes corresponding to 2θ values of 29.08°. The surface crystals of Mg-BC show the characteristic peaks of MgO (PDF No. 45–0946), with 2θ diffraction peaks appearing at 30.94° (111), 36.93° (111), 42.91° (200), 62.30° (220), and 76.00° (220). Moreover, $Mg(OH)_2$ crystals are detected at the main peak, and the sharp peak shape is consistent with the characteristic peaks of $Mg(OH)_2$ (PDF No. 07–0239). XPS could further reveal the elemental composition and valence states on the surfaces of the two materials. The XPS full spectra revealed that both BC and Mg-BC contained C, O, N, P, and Mg elements. This result indicated that sheep manure itself contained a small amount of Mg (Mg2p) (Fig. 3a). For C 1 s, after BC was

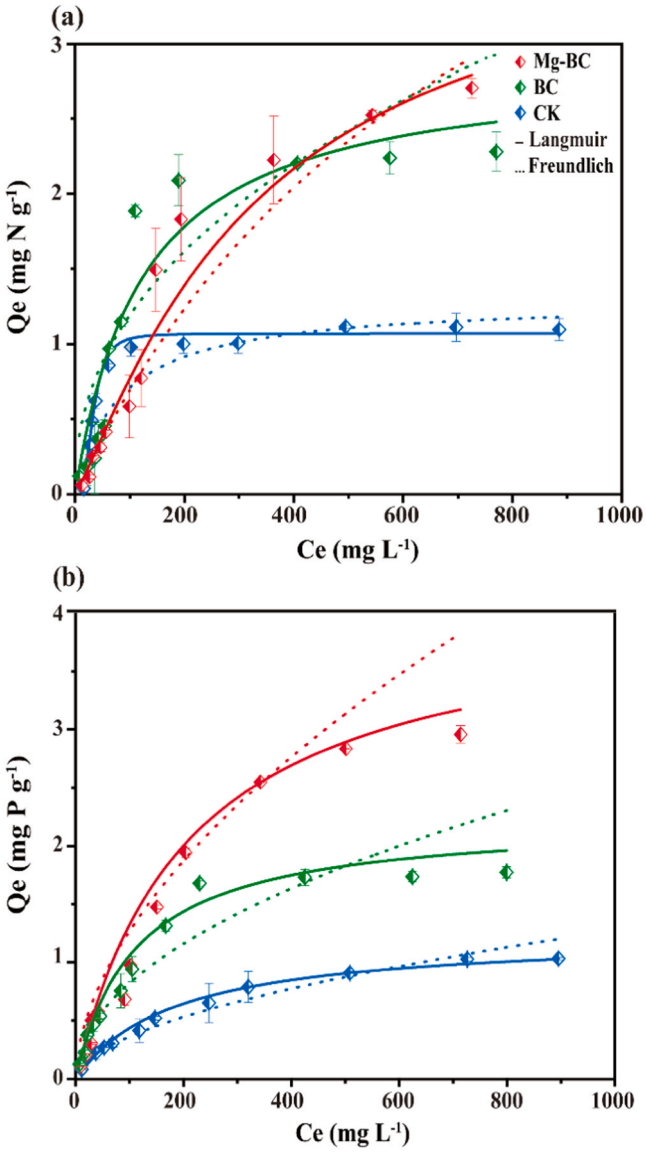

Fig. 4. (a) NO_3^- and (b) PO_4^{3-} adsorption isotherms of soils in dual-solute systems amended with Mg-BC (Mg-modified biochar) and BC (raw biochar).

modified, the peak area of C═O increased (Fig. 3b). In O 1 s, two characteristic peaks attributed to MgO (529.78 eV, 530.78 eV) obviously appeared in Mg-BC, and the OH (531.78 eV) shifted to 531.88 eV, indicating that Mg interacted with OH and was successfully loaded onto the biochar (Fig. 3c).

3.2. Adsorption of NO_3^- and PO_4^{3-} in soils amended with BC and Mg-BC

As illustrated in Fig. 4 and Table 2, the Langmuir model effectively aligned with the adsorption isotherm well (R^2=0.945–0.998). Compared to CK, both BC and Mg-BC treatments performed excellent adsorption capacity for nitrate and phosphate, with the Mg-BC treatment showing the highest adsorption capacity for NO_3^- at 3.96 mg g^{-1} and PO_4^{3-} at 4.11 mg g^{-1} . In addition, the maximum NO_3^- and PO_4^{3-} adsorption capacity of Mg-BC were 1.38 and 1.84 times those of BC treatment, respectively, and its PO_4^{3-} adsorption capacity was higher than that of NO_3^-.

3.3. Effects of BC and Mg-BC on Soil Leaching

3.3.1. N leaching from BC and Mg-BC amended soils

As shown in Fig. 5a, the content of TN in the leachate of different treatments first increased and then decreased over time. At day 6, the TN content in the leachate of CK, BC, and Mg-BC treatments reached the maximum value of 49.66, 36.88 and 31.88 mg L^{-1}, respectively. Throughout the leaching process, the TN content in the leachate of both BC and Mg-BC treatments remained lower than that of CK. In addition, compared to BC, the Mg-BC treatment significantly reduced the cumulative TN in leachate, DIN proportion, and NO_3^--N proportion by 30.98 %, 11.02 %, and 20.39 % ($P < 0.05$), respectively (Fig. 5b and c).

3.3.2. P leaching from BC and Mg-BC amended soils

As shown in Fig. 6a, the TP content in the leachate of CK, BC, and Mg-BC treatments reached the maximum value of 1.50, 1.09 and 0.99 mg L^{-1}, respectively, at day 12. On day 3, the TP content in the Mg-BC treatment was higher than that of the CK treatment, and then stayed lower than that of the CK. From day 9 onward, the TP content in the Mg-BC leachate was consistently lower than that of the BC treatment. Moreover, compared to BC, the Mg-BC treatment significantly reduced the cumulative TP and SRP proportion in the leachate by 51.25 % and 11.94 % ($P < 0.05$), respectively (Fig. 6b and c).

3.4. Soil available N and P content and pakchoi biomass in soils amended with BC and Mg-BC

As shown in Table 3, compared to CK, both BC and Mg-BC treatments significantly increased pakchoi biomass and nutrient uptake ($P < 0.05$). Furthermore, the Mg-BC treatment significantly enhanced biomass, N uptake, and K uptake by 17.28 %, 20.83 %, and 123.77 %, respectively, compared to BC ($P < 0.05$).

As shown in Fig. 7, both BC and Mg-BC treatments significantly increased soil TP, NO_3^--N, and AP contents compared to CK, with significant increases of 5.74 %–12.18 %, 73.52 %–296.01 %, and 8.06 %–31.25 % ($P < 0.05$), respectively. Moreover, compared to BC, the Mg-BC treatment significantly improved soil NO_3^--N, NH_4^+-N, TP, and AP contents by 128.22 %, 44.67 %, 6.09 %, and 52.94 % ($P < 0.05$), respectively. Whereas, the soil TN content of each treatment did not show significant differences.

4. Discussion

4.1. Characterization response of Mg-modified biochar

Numerous studies have employed Mg element for the functional modification of biochar (Oginni et al., 2020; Pinto et al., 2019; Samaraweera et al., 2023). In this study, scanning electron microscopy (SEM) images of sheep manure biochar (BC) revealed a relatively smooth surface (Fig. 1b), whereas after modification with Mg element, the sample surface became rougher, with white granular and needle-like substances attached to the pore surfaces and inner walls (Fig. 1a). These results were consistent with the findings of Wu et al. (2019), who attributed such differences to the presence of surface MgO. Additionally, FTIR analysis found that the

Table 2
Langmuir and Freundlich adsorption isotherm coefficients and the coefficient of determination (R^2) for the fit of data.

Solution	Treatment	Langmuir			Freundlich		
		K_L (L mg^{-1})	Q (mg g^{-1})	R_L^2	n	K_f (mg^{1-n} Ln g^{-1})·	R_F^2
NO_3^-	Mg-BC	0.0082	3.963	0.990	2.271	0.154	0.975
	BC	0.0184	2.869	0.945	4.333	0.110	0.939
	CK	0.0123	1.286	0.998	2.109	0.014	0.991
PO_4^{3-}	Mg-BC	0.0048	4.105	0.996	1.780	0.132	0.974
	BC	0.0090	2.233	0.980	2.018	0.096	0.893
	CK	0.0055	1.239	0.998	1.84	0.067	0.980

Notes: CK, no biochar; BC, raw biochar; Mg-BC, Mg-modified biochar.

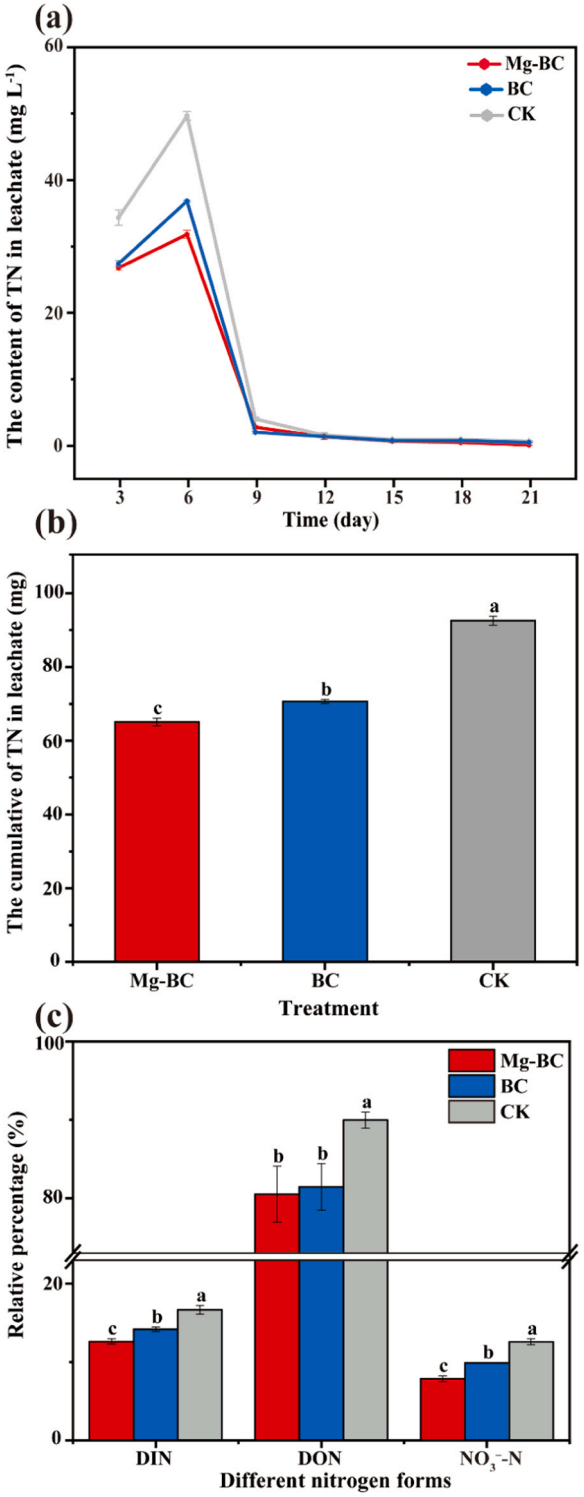

Fig. 5. (a) The contents of TN in leachate, (b) the cumulative of TN in leachate, and (c) the relative percentages of different N forms in leaching solution. CK, no biochar; BC, raw biochar; Mg-BC, Mg-modified biochar. Error bars represent standard error of the mean (n = 3) and lowercase letters indicate significant difference among the different treatments ($P < 0.05$). TN, total N; DIN, dissolved inorganic N; DON, dissolved organic N.

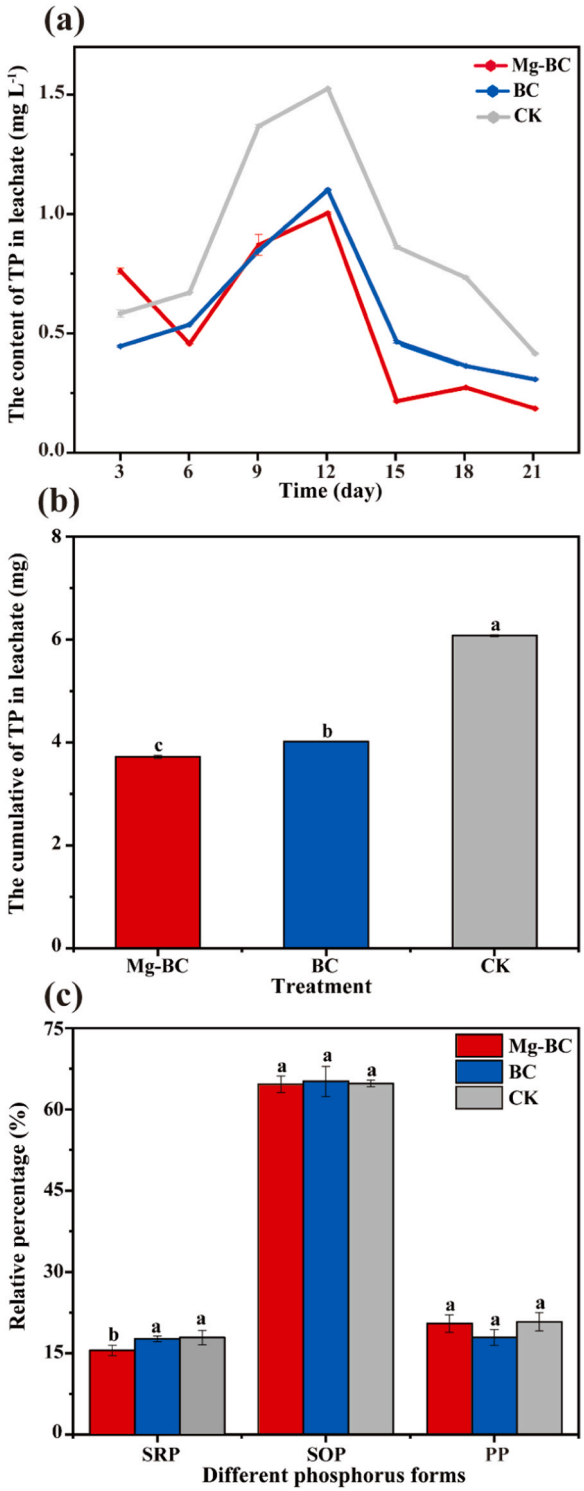

Fig. 6. (a) The contents of TP in leachate, (b) the cumulative of TP in leachate, and (c) the relative percentages of different P forms in leaching solution. CK, no biochar; BC, raw biochar; Mg-BC, Mg-modified biochar. Error bars represent standard error of the mean (n = 3) and lowercase letters indicate significant difference among the different treatments ($P < 0.05$). TP, total P; PP, paniculate P; SOP, soluble organic P; SRP, soluble reactive P.

Table 3
Effects of biochar on pot yield and N, P, and K content in pakchoi at harvest that was grown in a greenhouse vegetable soil.

Treatment	Yield (g pot^{-1})	N uptake (g pot^{-1})	P uptake (g pot^{-1})	K uptake (g pot^{-1})
Mg-BC	91.01 ± 5.88a	0.29 ± 0.01a	0.04 ± 0.01a	0.26 ± 0.03a
BC	77.60 ± 5.02b	0.24 ± 0.03b	0.03 ± 0.01ab	0.17 ± 0.04b
CK	67.62 ± 2.19c	0.20 ± 0.01b	0.02 ± 0.01b	0.12 ± 0.01c

Notes: Error bars represent standard error of the mean (n = 3) and lowercase letters indicate significant difference among the different treatments ($P < 0.05$). CK, no biochar; BC, raw biochar; Mg-BC, Mg-modified biochar.

peaks of Mg-BC at 1643 cm^{-1} (-COOH), 3413 cm^{-1} (-OH), and 3230 cm^{-1} (-C═O) were significantly enhanced, while a new peak appeared at 620 cm^{-1} , indicating the presence of an Mg-O bond (Fig. 2a). These results aligned with those of Yin et al. (2018) confirming the successful loading of Mg onto the biochar. Previous studies reported that Mg-BC contained more C-O, C═O, and COOH functional groups compared to BC (Chen et al., 2018). XRD analysis further confirmed the presence of characteristic diffraction peaks of Mg chloride in the Mg-BC, along with the crystal structures of MgO and $Mg(OH)_2$ (Fig. 2b). These findings were consistent with those of Zin and Kim (2021), indicating that after the successful loading of Mg onto the biochar, additional active adsorption sites (such as oxygen-containing functional groups and Mg-binding sites) formed on its surface. These newly introduced adsorption sites significantly enhanced the surface reactivity of the biochar, thereby exerting a substantial influence on its adsorption performance (Yin et al., 2018). In this study, XPS further confirmed that the peak area of C═O functional groups on the surface of Mg-BC increased (Fig. 3b), which was consistent with the previous report by Wang et al. (2024). In addition, a new peak attributed to Mg (Mg1s) appeared in the full scan spectrum, confirming that Mg had been successfully loaded onto the modified biochar. Compared to BC, OH shifted by 0.1 eV, indicating that Mg in Mg-BC might have interacted with OH to form Mg-O (Wang et al., 2024).

4.2. Response of NO_3^- and PO_4^{3-} adsorption to Mg-modified biochar

The adsorption data indicated that the Langmuir model better fitted the experimental results than the Freundlich model (Table 2), which is consistent with the adsorption results in aqueous solutions (Fig. S1 and Table S1). Our study on mixed aquatic solutions confirmed that chemisorption is the main mechanism by which biochar achieves the co-adsorption of NO_3^- and PO_4^{3-} (Fig. S2 and Table S2) , aligning with Tang et al. (2025). This was attributed to the fact that the adsorption of NO_3^- by biochar primarily involved monolayer homogeneous adsorption through chemical interactions, whereas the adsorption of PO_4^{3-} entailed both monolayer chemical adsorption and precipitation. Peng et al. (2021) also emphasized that chemical bonding is crucial for N/P adsorption, with chemical precipitation exhibiting stronger capacity and affinity than physical adsorption. In contrast, Ghodszad et al. (2022) found the Freundlich model provided a better fit for P adsorption by wheat straw biochar, attributing this to multilayer adsorption. Such discrepancies may stem from variations in soil type, biomass source, biochar pH, and pyrolysis temperature.

Mechanistically, the positive surface charge of Mg-BC enhances anion adsorption. This charge arises from two key features of Mg-BC: its MgO/$Mg(OH)_2$ crystal structure and oxygen-containing functional groups (e.g., -OH, -COOH). (Guo et al., 2025b; Li et al., 2024a). At high pyrolysis temperatures, $MgCl_2$ decomposition generates a porous structure and active sites (e.g., Mg-O bonds), which improve adsorption capacity (Li et al., 2016; Zhang et al., 2012). This study showed Mg-BC had 1.38 (NO_3^-) and 1.84 (PO_4^{3-}) times higher adsorption capacities than BC (Fig. 4 and Table 2), consistent with Tang et al. (2025). The superior performance of Mg-BC likely results from electrostatic attraction, chemical bonding, and precipitation via its MgO/$Mg(OH)_2$ crystals (Dai et al., 2020; Wu et al., 2019; Zheng et al., 2020).

Notably, NO_3^- and PO_4^{3-} competed for reactive sites on Mg-BC, with PO_4^{3-} exhibiting a higher maximum adsorption capacity (Table 2). Previous studies showed PO_4^{3-} significantly inhibits NO_3^- adsorption, while NO_3^- has minimal impact on PO_4^{3-} adsorption, possibly due to NO_3^-'s weaker competitive ability (Dai et al., 2020; Liu et al., 2010; Yao et al., 2013). However, Yao et al. (2013) found NO_3^- reduced PO_4^{3-} adsorption by tomato tissue-derived biochar, highlighting the role of raw material and pyrolysis conditions. Additionally, competition from other anions (e.g., HCO_3^-, SO_4^{2-}) and soil pH variations further influence N/P adsorption (Tang et al., 2025; Yao et al., 2013).

4.3. Response of N and P leaching to Mg-modified biochar

The findings of this research indicated that the TN content in the leachate of each treatment exhibited an initial rise followed by a subsequent decline with time (Fig. 5a). During the early stage (days 3–6), the TN content in the leachate was relatively high. This might be due to the rapid leaching of externally applied N fertilizer and the highly accumulated N in the facility soil with irrigation water (Dong et al., 2022). However, this differed from the findings of Zhou et al. (2024) in clay soil, where they believed that the TN concentration in the leachate decreased with an increase in leaching times. Such differences might be related to factors such as soil texture, nutrient content, and fertilization. For the change in TP content in the leachate (Fig. 6a), on day 3, the TP content in the leachate of the Mg-BC treatment exceeded those of the BC and CK treatments. This was analogous to the findings of Zheng et al. (2020), it is believed that the Mg compounds on the surface of Mg-BC formed soluble complexes (such as $MgHPO_4$ or $Mg(H_2PO_4)_2$) with P, which were more easily released into the leachate at the initial leaching stage, leading to an increase in P content. In addition, the TP content in the Mg-BC treatment showed concentration peaks on days 12 and 18. This revealed that Mg-BC reduced the rate of soil P

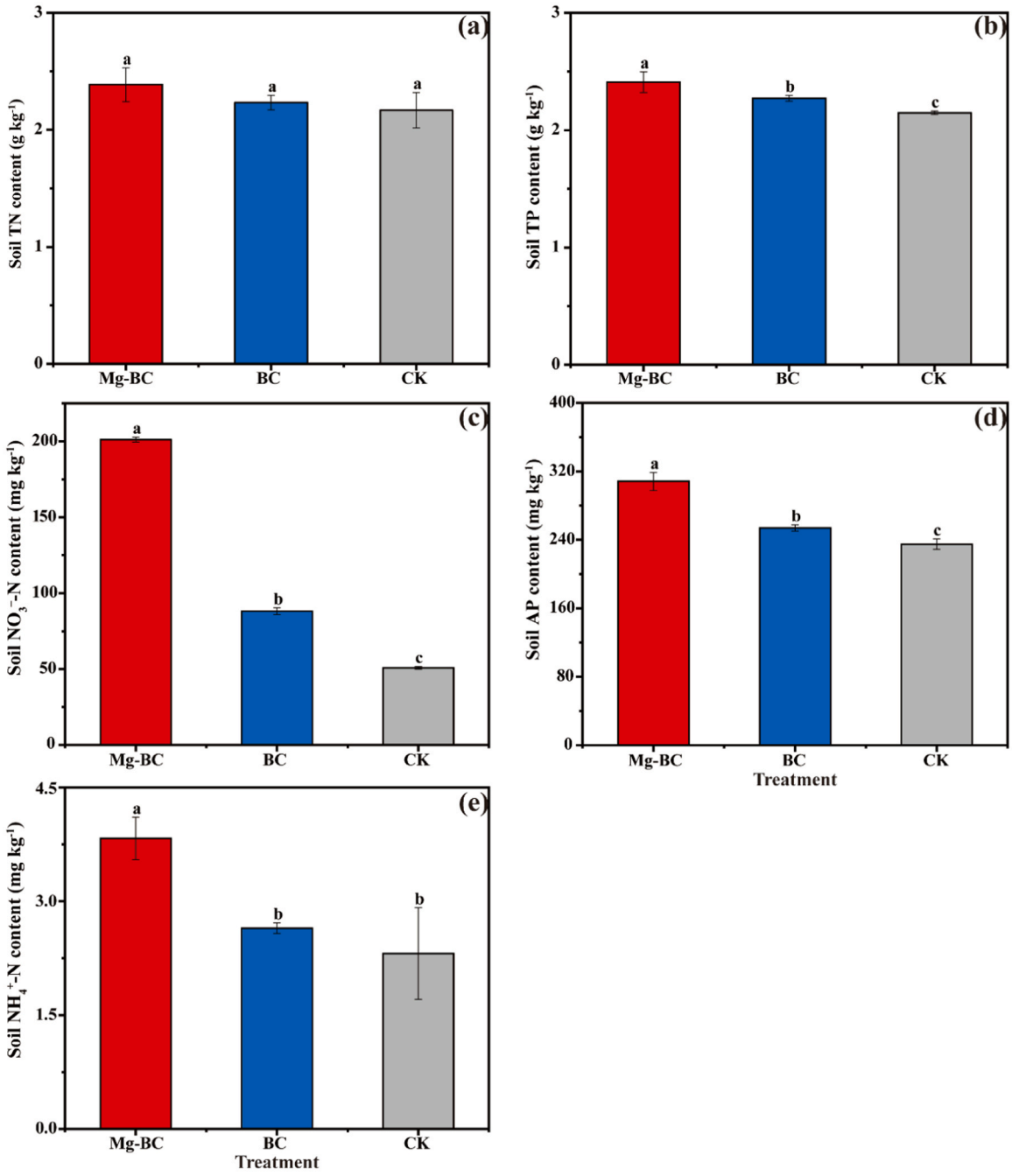

Fig. 7. Effects of biochar applications on (a) TN, (b) TP, (c) NO_3^--N, (d) AP, and (e) NH_4^+-N in pakchoi pot soil. Error bars represent standard error of the mean (n = 3) and lowercase letters indicate significant difference among the different treatments ($P < 0.05$). CK, no biochar; BC, raw biochar; Mg-BC, Mg-modified biochar; TN, total nitrogen; TP, total phosphorus; NO_3^--N, nitrate nitrogen; AP, available phosphorus; NH_4^+-N, ammonium nitrogen.

release and extended the retention duration of P in the soil through adsorption-desorption processes (Wu et al., 2019; Zheng et al., 2020).

The research revealed that the Mg-BC treatment significantly decreased the accumulation of TN and TP in the leachate compared to CK and BC (Fig. 5b and Fig. 6b). This was comparable to the results obtained by Zhou et al. (2024) and Zheng et al. (2020), indicating that Mg-BC performed well in reducing N and P leaching. The formation of the above phenomenon was mainly attributed to two reasons: (i) the surface of Mg-BC had many new active sites. These charged active sites generated strong electrostatic attraction with N and P nutrient ions, consequently, the material's ability to absorb N and P is greatly improved (Peng et al., 2022; Shrivastava et al.,

2024); (ii) the surface of Mg-BC contained more hydrophilic groups, leading to a substantial enhancement in the soil's ability to retain water (Yin et al., 2018). This reduced the loss of N and P through leaching with water. In addition, the contents of DIN, NO_3^--N, and SRP in the Mg-BC leachate were notably reduced compared to those in the BC and CK treatments (Fig. 5c and Fig. 6c). This finding aligns with the outcomes reported by Zhou et al. (2024) and Zheng et al. (2020), it was found that adding Mg-BC can effectively reduce the bioavailability of N and P in the leachate. This, in turn, reduces the potential risk of eutrophication in groundwater and lakes (Tang et al., 2025). Although soil column leaching could simulate short-term soil leaching processes under controlled conditions (e.g., temperature, humidity, leaching rate), it had certain limitations compared to leaching phenomena in long-term field environments (Guo et al., 2025a). Therefore, the mechanistic findings revealed by soil column leaching needed to be validated under field conditions to enhance the scientific rigor and persuasiveness of the research conclusions.

4.4. Response of Soil available N and P content and pakchoi biomass to Mg-modified biochar

In this research, compared to the CK and BC, the Mg-BC treatment increased the contents of TN, NO_3^--N, NH_4^+-N, TP, and AP in the soil (Fig. 7b, c, d, e). This further substantiated that Mg-BC not only augments the soil's capacity to retain N and P nutrients but also improve nutrient availability. This result matched the findings of Wu et al. (2020) and Wu et al. (2019), mainly attributed to two aspects: On one hand, the active adsorption sites formed by MgO and $Mg(OH)_2$ on the surface of Mg-BC gave it a specific adsorption advantage for N and P nutrients. The study also showed that it could continuously supply N and P to the soil by slowly releasing nutrients later (Wu et al., 2019). On the other hand, Mg-BC efficiently prevented the leaching depletion of N and P nutrients (Yin et al., 2018; Zhou et al., 2024), maintaining the nutrient storage capacity and thus improving their availability.

The study demonstrated that the concurrent use of Mg-BC and chemical fertilizers increased the nutrient content of pakchoi (Table 3), which was consistent with the conclusions of Wu et al. (2019). This was because Mg-BC could enhance soil nutrient retention through surface functional group complexation and pore adsorption (Wang et al., 2019). After the adsorption process in aquatic systems, $MgNH_4PO_4{\cdot}6H_2O$ was found on the surface of Mg-BC (Fig. S3). Its unique slow-release characteristics precisely match the dynamic nutrient release with the N and P demand during the pakchoi's growing period (Wu et al., 2016). This spatiotemporal coupling effect not only promoted the crop's periodic absorption and utilization of nutrients (Namatsheve et al., 2024), but also maintained soil fertility stability by reducing the risk of nutrient leaching. Additionally, Mg-BC treatment increased the biomass of pakchoi by 17.28 %, which is similar to the research results of Wu et al. (2019). This might be attributed to the fact that Mg-modified biochar enhanced nutrient availability, achieved synergistic optimization of nitrogen and phosphorus, promoted crop uptake, and thereby increased crop biomass.

5. Conclusion

This study demonstrated that Mg-modified biochar (Mg-BC) significantly enhanced the adsorption and interception capacity of NO_3^- and PO_4^{3-} in greenhouse vegetable soils. The results showed that Mg-BC exhibited abundant oxygen-containing functional groups and a unique crystalline structure, and its adsorption of NO_3^- and PO_4^{3-} was mainly characterized by chemical homogeneous monolayer adsorption, showing a particularly stronger affinity for PO_4^{3-} (maximum adsorption capacity of 4.11 mg g^{-1}). Compared to raw biochar (BC), Mg-BC more effectively reduced TN and TP leaching losses by 30.98 % and 51.25 %, effectively inhibiting the leaching of DIN, NO_3^--N, and SRP. Furthermore, Mg-BC treatment significantly improved soil N and P availability, while promoting nutrient uptake and biomass enhancement in pakchoi. These findings highlight the effectiveness of Mg-BC in increasing the likelihood of N and P adsorption and interception within the soil, as well as the nutrient supply capacity, which is of great significance for promoting the sustainable greenhouse vegetable production.

CRediT authorship contribution statement

Yuyang Cheng: Writing – original draft, Data curation. **He Wang:** Investigation, Data curation. **Zhengping Peng:** Writing – review & editing, Conceptualization. **Xinyue Wen:** Investigation, Formal analysis. **Yaling Wang:** Writing – review & editing, Writing – original draft, Data curation. **Xiuwen Mei:** Formal analysis, Data curation. **Chunjing Liu:** Writing – review & editing, Supervision, Project administration. **Wang Xubin:** Writing – review & editing, Supervision, Project administration, Funding acquisition.

Declaration of Competing Interest

The authors declare that they have no known competing financial interests or personal relationships that could have appeared to influence the work reported in this paper.

Acknowledgements

The work was financially supported by the National Natural Science Foundation of China (32272816), the Smart Fertilization Project (20221805), the National Key R&D Program of China (2022YFD1901300) and the Agricultural Science and Technology Innovation Program (No. CAAS-ZDRW202201).

Appendix A. Supporting information

Supplementary data associated with this article can be found in the online version at doi:10.1016/j.eti.2025.104423.

Data availability

Data will be made available on request.

References

Adelawon, B.O., Latinwo, G.K., Eboibi, B.E., Agbede, O.O., Agarry, S.E., 2021. Comparison of the slow, fast, and flash pyrolysis of recycled maize-cob biomass waste, box-benhken process optimization and characterization studies for the thermal fast pyrolysis production of bio-energy. Chem. Eng. Commun. 209 (9), 1246–1276. https://doi.org/10.1080/00986445.2021.1957851.

Ahmed, N., Tu, P., Deng, L., Chachar, S., Chachar, Z., Deng, L., 2024. Optimizing the dual role of biochar for phosphorus availability and arsenic immobilization in soils. Sci. Total Environ. 957, 177810. https://doi.org/10.1016/j.scitotenv.2024.177810.

Cao, Y., Wang, X., Bai, Z., Chadwick, D., Misselbrook, T., Sommer, G., Qin, S., Ma, L, W., 2019. Mitigation of ammonia, nitrous oxide and methane emissions during solid waste composting with different additives: a meta-analysis. J. Clean. Prod. 235, 626–635. https://doi.org/10.1016/j.jclepro.2019.06.288.

Chandra, S., Medha, I., Bhattacharya, J., 2020. Potassium-iron rice straw biochar composite for sorption of nitrate, phosphate, and ammonium ions in soil for timely and controlled release. Sci. Total Environ. 712, 136337. https://doi.org/10.1016/j.scitotenv.2019.136337.

Chen, Q., Qin, J., Cheng, Z., Huang, L., Sun, P., Chen, L., Shen, G., 2018. Synthesis of a stable magnesium-impregnated biochar and its reduction of phosphorus leaching from soil. Chemosphere 199, 402–408. https://doi.org/10.1016/j.chemosphere.2018.02.058.

Dai, Y., Wang, W., Lu, L., Yan, L., Yu, D., 2020. Utilization of biochar for the removal of nitrogen and phosphorus. J. Clean. Prod. 257, 120573. https://doi.org/10.1016/j.jclepro.2020.120573.

Datta, A., Shrestha, S., Ferdous, Z., Win, C.C., 2015. Strategies for enhancing phosphorus efficiency in crop production systems. Nutr. Use Effic. Basics Adv. Springe N. Delhi 59–71. https://doi.org/10.1007/978-81-3222169-2_5.

Dong, Y., Yang, J.-L., Zhao, X.-R., Yang, S.-H., Mulder, J., Dörsch, P., Zhang, G.-L., 2022. Nitrate leaching and n accumulation in a typical subtropical red soil with n fertilization. Geoderma 407, 115559. ⟨http://10.1016/j.geoderma.2021.115559⟩.

Fang, L., Li, J.-s, Donatello, S., Cheeseman, C.R., Poon, C.S., Tsang, D.C.W., 2020. Use of Mg/Ca modified biochars to take up phosphorus from acid-extract of incinerated sewage sludge ash (ISSA) for fertilizer application. J. Clean. Prod. 244, 118853. https://doi.org/10.1016/j.jclepro.2019.118853.

Freschet, G., Masse, D., Hien, E., Sall, S., Chotte, J., 2008. Long-term changes in organic matter and microbial properties resulting from manuring practices in an arid cultivated soil in Burkina Faso. Agric. Ecosyst. Environ. 123 (1-3), 175–184. https://doi.org/10.1016/j.agee.2007.05.012.

Ghodszad, L., Reyhanitabar, A., Oustan, S., Alidokht, L., 2022. Phosphorus sorption and desorption characteristics of soils as affected by biochar. Soil Tillage Res. 216, 105251. https://doi.org/10.1016/j.still.2021.105251.

Gong, Y., Hou, R., Fu, Q., Li, T., Wang, J., Su, Z., Shen, W., Zhou, W., Wang, Y., Li, M., 2024. Modified biochar reduces the greenhouse gas emission intensity and enhances the net ecosystem economic budget in black soil soybean fields. Soil Tillage Res. 237, 105978. https://doi.org/10.1016/j.still.2023.105978.

Gu, F., Han, S., Wang, H., Wang, Y., Ma, X., Li, L., 2023. Effect of metal ion-modified biochar on nitrogen adsorption and migration features of black soil. J. Northwest AF Univ. 51 (10), 97–106. https://doi.org/10.13207/j.cnki.jnwafu.2023.10.011.

Gu, X., Li, H., Shi, Y., Sun, C., Li, J., Li, S., 2025. Magnesium modified biochar facilitates favorable nitrogen conversion to mitigate ammonia and nitrous oxide emissions during pig manure composting. Chem. Eng. J. 504, 159073. https://doi.org/10.1016/j.cej.2024.159073.

Guo, R., Gong, W., Qi, S., Xu, J., Shang, Z., Joseph, S., 2025a. Biochar-based urea enhances nitrogen use efficiency and mitigates nitrogen leaching in greenhouse vegetable production. Environ. Technol. Innov. 38, 104104. https://doi.org/10.1016/j.eti.2025.104104.

Guo, Z., Zhang, D., Ma, L., Dai, Q., Yang, R., Ao, R., 2025b. Magnesium modified algae biochar for phosphorus adsorption: synthesis, experimental analysis, DFT calculations and regeneration. J. Water Process Eng. 71, 107169. https://doi.org/10.1016/j.jwpe.2025.107169.

Haefele, S.M., Konboon, Y., Wongboon, W., Amarante, S., Maarifat, A.A., Pfeiffer, E.M., Knoblauch, C., 2011. Effects and fate of biochar from rice residues in rice-based systems. Field Crops Res. 121 (3), 430–440. https://doi.org/10.1016/j.fcr.2011.01.014.

Ibrahim, M.M., Liu, D., Wu, F., Chen, Y., He, Z., Zhang, W., Xing, S., Mao, Y., 2023. Nitrogen retention potentials of magnesium oxide- and sepiolite-modified biochars and their impacts on bacterial distribution under nitrogen fertilization. Sci. Total Environ. 866, 161358. https://doi.org/10.1016/j.scitotenv.2022.161358.

Kalkhajeh, Y.K., Huang, B., Hu, W., Holm, P.E., Bruun Hansen, H.C., 2017. Phosphorus saturation and mobilization in two typical Chinese greenhouse vegetable soils. Chemosphere 172, 316–324. https://doi.org/10.1016/j.chemosphere.2016.12.147.

Kalkhajeh, Y.K., Huang, B., Hu, W., Ma, C., Gao, H., Thompson, M.L., Hansen, H.C.B., 2021. Environmental soil quality and vegetable safety under current greenhouse vegetable production management in China. Agric. Ecosyst. Environ. 307, 107230. https://doi.org/10.1016/j.agee.2020.107230.

Li, M., Xie, Q., Xu, F., Zhang, Y., Zhuang, Z., Xu, J., Xiang, H., Li, Y., Cai, Y., Chen, Z., Yu, B., 2024a. Screening of metal-modified biochars for practical phosphorus recovery. Sci. Total Environ. 956, 177342. https://doi.org/10.1016/j.scitotenv.2024.177342.

Li, R., Wang, J.J., Zhou, B., Awasthi, M.K., Ali, A., Zhang, Z., Gaston, L.A., Lahori, A.H., Mahar, A., 2016. Enhancing phosphate adsorption by Mg/Al layered double hydroxide functionalized biochar with different Mg/Al ratios. Sci. Total Environ. 559, 121–129. https://doi.org/10.1016/j.scitotenv.2016.03.151.

Li, S., Ma, X., Ma, Z., Dong, X., Wei, Z., Liu, X., zhu, L., 2021. Mg/Al-layered double hydroxide modified biochar for simultaneous removal phosphate and nitrate from aqueous solution. Environ. Technol. Innov. 23, 101771. https://doi.org/10.1016/j.eti.2021.101771.

Li, Y., Xu, Z., Zhang, L., Chen, W., Feng, G., 2024b. Dynamics between soil fixation of fertilizer phosphorus and biological phosphorus mobilization determine the phosphorus budgets in agroecosystems. Agric. Ecosyst. Environ. 375, 109174. https://doi.org/10.1016/j.agee.2024.109174.

Liu, H., Dong, Y., Wang, H., Liu, Y., 2010. Ammonium adsorption from aqueous solutions by strawberry leaf powder: equilibrium, kinetics and effects of coexisting ions. Desalination 263 (1-3), 70–75. https://doi.org/10.1016/j.desal.2010.06.040.

Macholdt, J., Piepho, H.-P., Honermeier, B., 2019. Mineral NPK and manure fertilisation affecting the yield stability of winter wheat: results from a long-term field experiment. Eur. J. Agron. 102, 14–22. https://doi.org/10.1016/j.eja.2018.10.007.

Mahmoud, M.E., Kamel, N.K., Amira, M.F., Fekry, N.A., 2024. Nitrate removal from wastewater by a novel co-biochar from guava seeds/beetroot peels-functionalized-Mg/Al double-layered hydroxide. Sep. Purif. Technol. 344, 127067. https://doi.org/10.1016/j.seppur.2024.127067.

Mehmood, K., Chang, S., Yu, S., Wang, L., Li, P., Li, Z., Liu, W., Rosenfeld, D., Seinfeld, J.H., 2017. Spatial and temporal distributions of air pollutant emissions from open crop straw and biomass burnings in China from 2002 to 2016. Environ. Chem. Lett. 16 (1), 301–309. https://doi.org/10.1007/s10311-017-0675-6.

Muema, F.M., Richardson, Y., Keita, A., Sawadogo, M., 2024. An interdisciplinary overview on biochar production engineering and its agronomic applications. Biomass.. Bioenergy 190, 107416. https://doi.org/10.1016/j.biombioe.2024.107416.

Namatsheve, T., Martinsen, V., Obia, A., Mulder, J., 2024. Grain yield and nitrogen cycling under conservation agriculture and biochar amendment in agroecosystems of sub-Saharan Africa. A meta-analysis. Agric. Ecosyst. Environ. 376, 109243. https://doi.org/10.1016/j.agee.2024.109243.

Oginni, O., Yakaboylu, G.A., Singh, K., Sabolsky, E.M., Unal-Tosun, G., Jaisi, D., Khanal, S., Shah, A., 2020. Phosphorus adsorption behaviors of MgO modified biochars derived from waste woody biomass resources. J. Environ. Chem. Eng. 8 (2), 103723. ⟨http://10.1016/j.jece.2020.103723⟩.

Peng, X., Ye, L.L., Wang, C.H., Zhou, H., Sun, B., 2011. Temperature- and duration-dependent rice straw-derived biochar: characteristics and its effects on soil properties of an ultisol in Southern China. Soil Tillage Res. 112 (2), 159–166. https://doi.org/10.1016/j.still.2011.01.002.
Peng, Y., Chen, Q., Guan, C.-Y., Yang, X., Jiang, X., Wei, M., Tan, J., Li, X., 2023. Metal oxide modified biochars for fertile soil management: effects on soil phosphorus transformation, enzyme activity, microbe community, and plant growth. Environ. Res. 231, 116258. https://doi.org/10.1016/j.envres.2023.116258.
Peng, Y., Sun, Y., Fan, B., Zhang, S., Bolan, N.S., Chen, Q., Tsang, D.C.W., 2021. Fe/Al (hydr)oxides engineered biochar for reducing phosphorus leaching from a fertile calcareous soil. J. Clean. Prod. 279, 123877. https://doi.org/10.1016/j.jclepro.2020.123877.
Peng, Y., Zhang, B., Guan, C.Y., Jiang, X., Tan, J., Li, X., 2022. Identifying biotic and abiotic processes of reversing biochar-induced soil phosphorus leaching through biochar modification with MgAl layered (hydr)oxides. Sci. Total Environ. 843, 157037. https://doi.org/10.1016/j.scitotenv.2022.157037.
Pinto, M.d.C.E., Silva, D.Dd, Gomes, A.L.A., Santos, R.M.Md, Couto, R.A.Ad, Novais, R.Fd, Constantino, V.R.L., Tronto, J., Pinto, F.G., 2019. Biochar from carrot residues chemically modified with magnesium for removing phosphorus from aqueous solution. J. Clean. Prod. 222, 36–46. https://doi.org/10.1016/j.jclepro.2019.03.012.
Qin, X., Cheng, S., Xing, B., Xiong, C., Yi, G., Shi, C., Xia, H., Zhang, C., 2023. Preparation of high-efficient MgCl2 modified biochar toward Cd(II) and tetracycline removal from wastewater. Sep. Purif. Technol. 325, 124625. https://doi.org/10.1016/j.seppur.2023.124625.
Riddle, M., Cederlund, H., Schmieder, F., Bergström, L., 2018. Magnetite-coated biochar as a soil phosphate filter: from laboratory to field lysimeter. Geoderma 327, 45–54. ⟨http://10.1016/j.geoderma.2018.04.025⟩.
Samaraweera, H., Palansooriya, K.N., Dissanayake, P.D., Khan, A.H., Sillanpää, M., Mlsna, T., 2023. Sustainable phosphate removal using Mg/Ca-modified biochar hybrids: current trends and future outlooks. Case Stud. Chem. Environ. Eng. 8, 100528. ⟨http://10.1016/j.cscee.2023.100528⟩.
Shrivastava, A., Abhishek, K., Gupta, A.K., Jain, H., Kumari, M., Patel, M., Sharma, P., 2024. Removal of micro- and nano-plastics from aqueous matrices using modified biochar – a review of synthesis, applications, interaction, and regeneration. J. Hazard. Mater. Adv. 16, 100518. https://doi.org/10.1016/j.hazadv.2024.100518.
Sui, J., Dai, Y., 2025. Analysis of conservation practices for black soil based on organic matter and nitrogen contents in the black soil region of Northeast China. Sci. Rep. 15 (1), 23989. https://doi.org/10.1038/s41598-025-09426-9.
Sun, C., Cao, H., Huang, C., Wang, P., Yin, J., Liu, H., Tian, H., Xu, H., Zhu, J., Liu, Z., 2022. Eggshell based biochar for highly efficient adsorption and recovery of phosphorus from aqueous solution: kinetics, mechanism and potential as phosphorus fertilizer. Bioresour. Technol. 362, 127851. https://doi.org/10.1016/j.biortech.2022.127851.
Sun, X., Yang, X., Hu, Z., Liu, F., Xie, Z., Li, S., Wang, G., Li, M., Sun, Z., Bol, R., 2024. Biochar effects on soil nitrogen retention, leaching and yield of perennial citron daylily under three irrigation regimes. Agric. Water Manag. 296, 108788. https://doi.org/10.1016/j.agwat.2024.108788.
Tang, Y., Zhang, X., Yang, Q., Yan, Y., Ding, W., Du, W., Hu, F., Geng, Z., Xu, Cy, 2025. Enhanced removal of the ammonium, nitrate and phosphate by biochars derived from apple tree branches via different modification methods. Sep. Purif. Technol. 362, 131740. ⟨http://10.1016/j.seppur.2025.131740⟩.
Wang, J., Tu, X., Zhang, H., Cui, J., Ni, K., Chen, J., Cheng, Y., Zhang, J., Chang, S.X., 2020. Effects of ammonium-based nitrogen addition on soil nitrification and nitrogen gas emissions depend on fertilizer-induced changes in ph in a tea plantation soil. Sci. Total Environ. 747, 141340. https://doi.org/10.1016/j.scitotenv.2020.141340.
Wang, K., Wang, S., Zhang, X., Wang, W., Wang, X., Kong, F., Xi, M., 2024. The amelioration and improvement effects of modified biochar derived from spartina alterniflora on coastal wetland soil and suaeda salsa growth. Environ. Res. 240, 117426. https://doi.org/10.1016/j.envres.2023.117426.
Wang, Y., Villamil, M.B., Davidson, P.C., Akdeniz, N., 2019. A quantitative understanding of the role of co-composted biochar in plant growth using meta-analysis. Sci. Total Environ. 685, 741–752. https://doi.org/10.1016/j.scitotenv.2019.06.244.
Wei, B., Zhang, D., Jeyakumar, P., Trakal, L., Wang, H., Sun, K., Wei, Y., Zhang, X., Ling, H., He, S., Wu, H., Huang, Z., Li, C., Wang, Z., 2024. Iron-modified biochar effectively mitigates arsenic-cadmium pollution in paddy fields: a meta-analysis. J. Hazard. Mater. 469, 133866. https://doi.org/10.1016/j.jhazmat.2024.133866.
Wei, K., Bao, H., Huang, S., Chen, L., 2017. Effects of long-term fertilization on available P, p composition and phosphatase activities in soil from the Huang-Huai-Hai plain of China. Agric. Ecosyst. Environ. 237, 134–142. https://doi.org/10.1016/j.agee.2016.12.030.
Weng, Z., Van Zwieten, L., Singh, B.P., Tavakkoli, E., Kimber, S., Morris, S., Macdonald, L.M., Cowie, A., 2018. The accumulation of rhizodeposits in organo-mineral fractions promoted biochar-induced negative priming of native soil organic carbon in ferralsol. Soil Biol. Biochem. 118, 91–96. https://doi.org/10.1016/j.soilbio.2017.12.008.
Wu, H., Zhang, Y., Yuan, Z., Gao, L., 2016. Phosphorus flow management of cropping system in huainan, China, 1990–2012. J. Clean. Prod. 112, 39–48. https://doi.org/10.1016/j.jclepro.2015.06.078.
Wu, L., Wei, C., Zhang, S., Wang, Y., Kuzyakov, Y., Ding, X., 2019. MgO-modified biochar increases phosphate retention and rice yields in saline-alkaline soil. J. Clean. Prod. 235, 901–909. https://doi.org/10.1016/j.jclepro.2019.07.043.
Wu, L., Zhang, S., Wang, J., Ding, X., 2020. Phosphorus retention using iron (II/III) modified biochar in saline-alkaline soils: adsorption, column and field tests. Environ. Pollut. 261, 114223. https://doi.org/10.1016/j.envpol.2020.114223.
Wu, L., Xu, D., Li, B., Wu, D., Yang, H., 2024. Enhanced removal efficiency of nitrogen and phosphorus from swine wastewater using MgO modified pig manure biochar. J. Environ. Chem. Eng. 12 (1), 111793. https://doi.org/10.1016/j.jece.2023.111793.
Xu, G., Zhang, Y., Sun, J., Shao, H., 2016. Negative interactive effects between biochar and phosphorus fertilization on phosphorus availability and plant yield in saline sodic soil. Sci. Total Environ. 568, 910–915. https://doi.org/10.1016/j.scitotenv.2016.06.079.
Yao, Y., Gao, B., Chen, J., Yang, L., 2013. Engineered biochar reclaiming phosphate from aqueous solutions: mechanisms and potential application as a Slow-Release fertilizer. Environ. Sci. Technol. 47 (15), 8700–8708. https://doi.org/10.1021/es4012977.
Yin, Q., Wang, R., Zhao, Z., 2018. Application of Mg–Al-modified biochar for simultaneous removal of ammonium, nitrate, and phosphate from eutrophic water. J. Clean. Prod. 176, 230–240. https://doi.org/10.1016/j.jclepro.2017.12.117.
Zhang, C., Huang, X., Zhang, X., Wan, L., Wang, Z., 2021. Effects of biochar application on soil nitrogen and phosphorous leaching loss and oil peony growth. Agric. Water Manag. 255, 107022. https://doi.org/10.1016/j.agwat.2021.107022.
Zhang, G., Zhang, L., Shi, Z., Yang, Y., Liu, J., 2025a. Microbial nutrient limitation and carbon use efficiency in saline-alkali soil amended with biochar: insights from ecoenzymatic C:N:P stoichiometry. Biochar 7 (1), 68. https://doi.org/10.1007/s42773-025-00458-y.
Zhang, J., Sun, H., Ma, J., Zhang, X., Wang, C., Zhou, S., 2023. Effect of straw biochar application on soil carbon, greenhouse gas emissions and nitrogen leaching: a vegetable crop rotation field experiment. Soil Use Manag. 39 (2), 729–741. https://doi.org/10.1111/sum.12877.
Zhang, M., Gao, B., Yao, Y., Xue, Y., Inyang, M., 2012. Synthesis of porous MgObiochar nanocomposites for removal of phosphate and nitrate from aqueous solutions. Chem. Eng. J. 210, 6–32. https://doi.org/10.1016/j.cej.2012.08.052.
Zhang, X., Wu, M., Liu, Z., Ou, Y., Zhang, T., Li, M., 2025b. Comprehensive effects of biochar-assisted nitrogen and phosphorus bioremediation on hydrocarbon removal and microecological improvement in petroleum-contaminated soil. Bioresour. Technol. 418, 131852. https://doi.org/10.1016/j.biortech.2024.131852.
Zheng, Q., Yang, L., Song, D., Zhang, S., Wu, H., Li, S., Wang, X., 2020. High adsorption capacity of Mg–Al-modified biochar for phosphate and its potential for phosphate interception in soil. Chemosphere 259, 127469. https://doi.org/10.1016/j.chemosphere.2020.127469.
Zhou, Y., Chen, Z., Zhao, Z., Wu, L., Wang, Y., Yang, J., An, N., Jing, H., 2024. Effects of magnesium-modified biochar on soil nitrogen leaching and growth of Chinese cabbage. J. Soils Sediment. 24 (6), 2318–2333. https://doi.org/10.1007/s11368-024-03793-y.
Zin, M.M.T., Kim, D.J., 2021. Simultaneous recovery of phosphorus and nitrogen from sewage sludge ash and food wastewater as struvite by Mg-biochar. J. Hazard. Mater. 403, 123704. https://doi.org/10.1016/j.jhazmat.2020.123704.